Journal of Computational Physics **179,** 371–399 (2002)
doi:10.1006/jcph.2002.7060

A Vortex Particle Method for Two-Dimensional Compressible Flow

Jeff D. Eldredge,[1] Tim Colonius, and Anthony Leonard

Division of Engineering and Applied Science, California Institute of Technology, Pasadena, California 91125
E-mail: jde26@eng.cam.ac.uk, colonius@caltech.edu, and tony@galcit.caltech.edu

Received April 26, 2001; revised March 5, 2002

A vortex particle method is developed for simulating two-dimensional, unsteady compressible flow. The method uses the Helmholtz decomposition of the velocity field to separately treat the irrotational and solenoidal portions of the flow, and the particles are allowed to change volume to conserve mass. In addition to having vorticity and dilatation properties, the particles also carry density, enthalpy, and entropy. The resulting evolution equations contain terms that are computed with techniques used in some incompressible methods. Truncation of unbounded domains via a nonreflecting boundary condition is also considered. The fast multipole method is adapted to compressible particles in order to make the method computationally efficient. The new method is applied to several problems, including sound generation by corotating vortices and generation of vorticity by baroclinic torque.

Key Words: vortex methods; Lagrangian methods; compressible flow; aeroacoustics.

1. INTRODUCTION

The Lagrangian nature of incompressible vortex particle methods makes them an interesting alternative to fixed-grid computational schemes such as finite-difference and spectral methods. Our motivation lies in exploiting their properties, to the maximum extent possible, for compressible flows, including those involving sound generation.

The importance of vorticity in sound generation has been established by many investigators. Chu and Kovásznay [7] presented an analysis of the higher order interactions between the three basic modes of fluctuation in the linearized equations of motion: the entropy mode, the vortical mode, and the acoustic mode. Their analysis clearly exhibited the importance of vorticity–vorticity and vorticity–acoustic interactions in the generation and processing of sound. Powell [40] isolated a dipole-like term involving the vorticity on the right-hand

[1] Present address: Department of Engineering, Cambridge University, Cambridge CB2 1PZ, UK.

0021-9991/02 $35.00

side of an acoustic analogy. Howe [23] recast the equations in a different form, using the stagnation enthalpy as the acoustic variable, thereby retaining the dipole source of Powell but without the density. Möhring [32] attempted to circumvent the difficulties associated with a source term that required knowledge of both the local vorticity and the velocity by forming an expression that was linear in the vorticity (and hence linear in the velocity). For flows of low Mach number, his formula provides knowledge of the acoustic far field based on the vorticity alone. Clearly a numerical method which emphasizes the motion of vorticity in a compressible medium can be used to further explore, and possibly exploit, the relationship between vorticity and sound. Furthermore, the present method will inherently decouple the velocity into irrotational and solenoidal components; these can be exploited in an acoustic investigation.

The development and application of incompressible vortex methods are described in several detailed reviews [29, 43] and a recent book by Cottet and Koumoutsakos [9]. We utilize several recent developments in incompressible vortex methods to make the extension to compressible flows. These include the deterministic method for the treatment of diffusion developed by Degond and Mas-Gallic [12], now referred to as particle strength exchange (PSE). As we show in [14], PSE also furnishes a useful framework for treating other physical phenomena, such as wave propagation. The expensive summation operation that once prohibited simulations of particle systems involving more than a few thousand particles has been alleviated with the development of fast methods, such as the fast multipole method of Greengard and Rokhlin [21]. These methods reduce the number of direct particle–particle interactions by computing interactions between clusters of particles where possible.

Particle methods have been used previously in the context of compressible flows. The method of smoothed particle hydrodynamics (SPH), first introduced by Gingold and Monaghan [19, 34], was originally used for astrophysical fluid dynamic applications. It relies on the same principle of kernel estimation as used by vortex methods, although it focuses on the velocity as the primary variable instead of the vorticity. Since its conception SPH has been used in several contexts outside of astrophysics: Monaghan and Gingold [37], and later Monaghan [36], applied the method to a shock-tube simulation using a special artificial viscosity to suppress spurious oscillations. The method has also been used for computing the Rayleigh–Taylor instability [35] and for blast waves. Anderson [3] developed a vortex method for flows in which the fluctuations in the density are small enough that the Boussinesq approximation is applicable. His method avoids computing the density gradient in the external force term by tracking this quantity directly rather than the density itself. The transport-element method developed by Krishnan and Ghoniem [26] is an extension of this approach, except that it uses the observation that the density gradient in such a flow is proportional to the length of a material line element or, alternatively, the distance between neighboring computational elements. The method has been applied to the Rayleigh–Taylor instability [26] and to the investigation of combustion in shear layers [45].

Research in combustion and reacting flows has led to advances in the capabilities of vortex methods when compressibility effects are present, some of which are evident in the present method. Ghoniem, Chorin, and Oppenheim [18] used the random vortex method [6] in conjunction with a flame propagation algorithm to study combustion. Though thermal effects are neglected in their vorticity evolution, the fluid dilatation behind the flame front is accounted for in the velocity field by using regularized volume sources collocated with the vortex particles, a technique that will be employed in the present work. Quackenbush *et al.* [41] developed a vortex method in which the density and reacting components are

transported by the particles along with the vorticity. The particle volumes are allowed to change to conserve mass, which is a crucial element of the present method. The baroclinic term in their method is accounted for through a "Lagrangian" reformulation, using the material derivative of the velocity in place of the pressure gradient. By assuming low Mach number, they allow the density to change only with temperature, thus simplifying the particle equations. Finally, Daeninck and Winckelmans [11] have computed nonisothermal incompressible flows by tracking the temperature along with the vorticity.

Sound generation has also been explored using incompressible vortex methods. Knio, Collorec, and Juvé [24] explored the sound emission from a complex system of vortices by simulating their motion in an incompressible medium and then computing the far-field sound using both the Powell–Hardin formulation and the Möhring analogy. Pothou and co-workers [39] used both the vortex particle and the vortex filament methods for three-dimensional simulations; they calculated the resulting acoustic field with acoustic analogies. Both of these investigations relied on the assumption of low Mach number to ignore compressibility effects in the flow region.

The present method does not rely on a low Mach number assumption. Inevitably some of the strength of vortex methods is compromised when applied to general compressible flows. Because the computational elements will carry radiating quantities in addition to vorticity, the region that they fill will necessarily be larger. But incompressible simulations that include viscosity require a surrounding buffer of particles with zero vorticity that accept the diffused quantity; in the present method waves will be allowed to propagate by the same principle and thus particle coverage need not be significantly larger, especially if sufficiently general boundary conditions may be developed. We propose a simple, but limited, technique in the present work.

The compressible method, which we refer to as the dilating vortex particle method (DVPM), is developed progressively, relying on existing techniques where possible. In Section 2 the Helmholtz decomposition of the velocity field will allow incorporation of the dilatation of fluid elements into the determination of the velocity. Computational elements that expand and contract according to the dilatation are introduced in this section, as well as a set of equations governing their strengths based on the compressible equations of motion. Domain truncation is dealt with in Section 3; a scheme based on Engquist and Majda's local boundary conditions [15] is described using the one-sided derivative treatment developed in [14]. In Section 4 other points for practical implementation are discussed, including the adaptations of the fast summation method and particle remeshing. Finally, the method is demonstrated on two model problems in Section 5. Conclusions and future extensions of the method are discussed in Section 6.

2. METHOD DESCRIPTION

2.1. *Velocity Decomposition*

Consider the Helmholtz decomposition of the velocity field, $\mathbf{u} = \mathbf{u}_s + \mathbf{u}_{ir}$, where $\mathbf{u}_s \equiv \nabla \times \mathbf{A}$, $\mathbf{u}_{ir} \equiv \nabla\varphi$, and $\mathbf{A}$ is chosen to be solenoidal. Taking the curl and the divergence of this relation leads to, respectively,

$$\begin{aligned} \nabla^2\mathbf{A} &= -\nabla \times \mathbf{u} \equiv -\boldsymbol{\omega}, \\ \nabla^2\varphi &= \nabla \cdot \mathbf{u} \equiv \theta. \end{aligned} \tag{1}$$

From hereon the flow is assumed to be two-dimensional, so the vorticity and the vector potential each have only a single component: $\boldsymbol{\omega} = \omega \hat{\mathbf{e}}_3$ and $\mathbf{A} = \psi \hat{\mathbf{e}}_3$. Equations (1) will be solved using the two-dimensional Green's function for the negative Laplacian, $G = -\frac{1}{2\pi} \log |\mathbf{x}|$. This inversion produces expressions for the potentials (within arbitrary constants)

$$\begin{aligned} \mathbf{A} &= G \star \boldsymbol{\omega}, \\ \varphi &= -G \star \theta, \end{aligned} \tag{2}$$

where $\star$ denotes convolution. If present, an extra irrotational, solenoidal component could be added to either expression; it will be ignored here. Substitution of these expressions into the velocity decomposition above leads to a relation for the velocity in terms of the vorticity and dilatation

$$\mathbf{u} = (\mathbf{K}\times) \star \boldsymbol{\omega} - \mathbf{K} \star \theta, \tag{3}$$

where

$$\mathbf{K}(\mathbf{x}) \equiv \nabla G(\mathbf{x}) = -\frac{\mathbf{x}}{2\pi |\mathbf{x}|^2}. \tag{4}$$

The first term on the right-hand side of (3) is the Biot–Savart integral, and the second is its counterpart in dilatation.

In a traditional vortex particle method the vorticity field is approximated (interpolated) by a set of regularized particles, or "blobs," each of which possesses its own distribution of vorticity

$$\tilde{\omega}(\mathbf{x}, t) = \sum_p \Gamma_p(t) \zeta_\varepsilon(\mathbf{x} - \mathbf{x}_p(t)), \tag{5}$$

where $\Gamma_p = V_p \omega_p$, $\omega_p = \omega(\mathbf{x}_p)$, V_p is the particle volume, ζ_ε is the blob function scaled by ε, the radius of the blob $\zeta_\varepsilon(\mathbf{x}) = \zeta(\mathbf{x}/\varepsilon)/\varepsilon^2$, and $\mathbf{x}_p$ is the particle position. The particles are material elements and thus their positions change according to the local fluid velocity:

$$\frac{d\mathbf{x}_p}{dt} = \mathbf{u}(\mathbf{x}_p). \tag{6}$$

The approximation (5) is introduced to the velocity expression (3) to account for the rotational contribution. However, the velocity field is not completely specified without the dilatation, so in the present method the particles will also carry the quantity

$$\tilde{\theta}(\mathbf{x}, t) = \sum_p Q_p(t) \zeta_\varepsilon(\mathbf{x} - \mathbf{x}_p(t)), \tag{7}$$

where $Q_p = V_p \theta_p$ and $\theta_p = \theta(\mathbf{x}_p)$. The regular distribution of these quantities serves to desingularize the velocity kernels [6]. Thus, the ODE that governs the particle positions is

$$\frac{d\mathbf{x}_p}{dt} = \sum_q \Gamma_q(t) \mathbf{K}_\varepsilon(\mathbf{x}_p - \mathbf{x}_q) \times \hat{\mathbf{e}}_3 - \sum_q Q_q(t) \mathbf{K}_\varepsilon(\mathbf{x}_p - \mathbf{x}_q), \tag{8}$$

where $\mathbf{K}_\varepsilon = \mathbf{K} \star \zeta_\varepsilon$ is the smoothed velocity kernel. Such a formula that accounts for contributions from both vorticity and fluid dilatation has been used previously in particle methods

[18, 41]. Accounting for the radial symmetry of the blob function, we obtain

$$\mathbf{K}_\varepsilon(\mathbf{x}) = -\frac{\mathbf{x}}{2\pi|\mathbf{x}|^2} q(|\mathbf{x}|/\varepsilon), \tag{9}$$

where $q(r) \equiv 2\pi \int_0^r \tau\zeta(\tau)\, d\tau$. Equation (8) exhibits the collaborative character of the vortex method. Each particle "induces" a velocity relative to it that is part azimuthal and part radial. The superposition of all of the particles' contributions defines the velocity field to which each particle is subjected.

The convergence of the incompressible vortex blob method has been demonstrated by Hald [22] and later by Beale and Majda [4], Raviart [42], and Anderson and Greengard [2]. In each it is shown that the errors in the method arise because of the smoothing of the velocity kernel and the discretization of the vorticity field by particles. A necessary constraint for convergence is that the particles overlap; i.e., the ratio of blob radius to particle spacing, $\kappa = \varepsilon/\Delta x$, must be greater than unity. In the present method, no additional errors have been introduced by including the dilatational component in the velocity field. The smoothing error is determined by the choice of blob function ζ; the order of accuracy r is dependent upon ζ satisfying a set of conditions on its moments,

$$\begin{aligned} \int \zeta(\mathbf{x})\, d\mathbf{x} &= 1, \\ \int x_1^{\alpha_1} x_2^{\alpha_2} \zeta(\mathbf{x})\, d\mathbf{x} &= 0, \quad |\alpha| \in [1, r-1], \end{aligned} \tag{10}$$

where $\alpha = (\alpha_1, \alpha_2)$ is a multi-index and $|\alpha| = \alpha_1 + \alpha_2$. We refer the reader to [5, 47] for a more complete discussion of the construction of the blob function. The construction is very similar to that of PSE kernels and interpolation kernels (see [14] and Section 4.2). In our implementation we use a Gaussian template (Eq. (28)). The second-order-accurate function derived from this template is the commonly used Gaussian $\zeta(\mathbf{x}) = \frac{1}{\pi} e^{-|\mathbf{x}|^2}$. With this choice the smoothed velocity kernel becomes

$$\mathbf{K}_\varepsilon(\mathbf{x}) = -\frac{\mathbf{x}}{2\pi|\mathbf{x}|^2}\left(1 - e^{-|\mathbf{x}|^2/\varepsilon^2}\right). \tag{11}$$

However, we use a higher order accurate function for our applications, as described in Section 5.

2.2. *Equations of Motion*

For Eq. (8) to be useful, the values of the vorticity and dilatation of every particle must be known. A set of equations that governs their evolution is developed by taking the curl and divergence of the momentum equations, respectively. For simplicity, the medium is assumed to be a calorically perfect monatomic gas. The properties (i.e., the dynamic viscosity, thermal conductivity, and specific heats) are assumed constant and uniform, which is valid in the absence of large temperature variations. The bulk viscosity is neglected—acceptable for a nonreacting monatomic gas [27]—although it can easily be introduced. In addition to the vorticity and dilatation, the flow is described by the specific enthalpy h, the specific entropy s, and the density ρ. Although only two variables are needed, the equations have a more compact form when expressed in terms of these three variables. The particle representations

of these variables are

$$\tilde{f}(\mathbf{x}, t) = \sum_p V_p f_p \zeta_\varepsilon(\mathbf{x} - \mathbf{x}_p(t)), \tag{12}$$

where f is either h, s, or ρ. The variables are made dimensionless with a typical acoustic scaling, using a characteristic flow length L, the speed of sound of the stagnant medium a_∞, the ambient density ρ_∞, the dynamic viscosity μ, and the specific heat capacity at constant pressure c_p, such that

$$\begin{aligned}
\tilde{x} &= x/L, & \tilde{u} &= u/a_\infty, & \tilde{\omega} &= \omega L/a_\infty, \\
\tilde{t} &= a_\infty t/L, & \tilde{\theta} &= \theta L/a_\infty, & \tilde{h} &= h/a_\infty^2, \\
\tilde{s} &= (s - s_\infty)/c_p, & \tilde{\rho} &= \rho/\rho_\infty, & \tilde{a}^2 &= a^2/a_\infty^2, \\
\tilde{T} &= c_p T/a_\infty^2, & \tilde{\Phi} &= \Phi L^2/(\mu a_\infty^2).
\end{aligned}$$

This scaling naturally leads to an acoustic definition of the Reynolds number, $Re = \rho_\infty a_\infty L/\mu$, which can be related to a hydrodynamic definition through a characteristic Mach number: $\widetilde{\mathrm{Re}} = M_0\, Re$, where $M_0 = U_0/a_\infty$ and U_0 is a typical flow velocity. The Prandtl number is $Pr = \mu c_p/k$, where k is the thermal conductivity. Note that, because the medium is a perfect gas, the temperature and the enthalpy are equivalent after nondimensionalization.

We begin with the momentum equation in dimensionless form (where the tildes have been removed for brevity),

$$\frac{\partial \mathbf{u}}{\partial t} + \mathbf{u}\cdot\nabla\mathbf{u} + \nabla h = T\nabla s + \frac{1}{Re}\frac{1}{\rho}\left(\frac{1}{3}\nabla\theta + \nabla^2\mathbf{u}\right). \tag{13}$$

We now express the viscous terms in a slightly different form to emphasize their dependence on the vorticity and dilatation, using the identity $\nabla^2\mathbf{u} = \nabla(\nabla\cdot\mathbf{u}) - \nabla\times\nabla\times\mathbf{u}$:

$$\frac{\partial \mathbf{u}}{\partial t} + \mathbf{u}\cdot\nabla\mathbf{u} + \nabla h = T\nabla s + \frac{1}{Re}\frac{1}{\rho}\left(\frac{4}{3}\nabla\theta - \nabla\times\boldsymbol{\omega}\right). \tag{14}$$

Taking the curl and divergence of this equation, respectively, results in the set of equations for the vorticity and dilatation

$$\frac{D\boldsymbol{\omega}}{Dt} = -\boldsymbol{\omega}\theta + \boldsymbol{\omega}\cdot\nabla\mathbf{u} + \nabla\times(h\nabla s) + \frac{1}{Re}\nabla\times\left[\frac{1}{\rho}\left(\frac{4}{3}\nabla\theta - \nabla\times\boldsymbol{\omega}\right)\right], \tag{15a}$$

$$\frac{D\theta}{Dt} = -\nabla^2 h - \nabla\mathbf{u} : (\nabla\mathbf{u})^T + \nabla\cdot(h\nabla s) + \frac{1}{Re}\nabla\cdot\left[\frac{1}{\rho}\left(\frac{4}{3}\nabla\theta - \nabla\times\boldsymbol{\omega}\right)\right]. \tag{15b}$$

Note that in two-dimensional flow, the vortex-stretching term (the second term on the right-hand side of (15a)) vanishes. We use the entropy form of the energy equation,

$$\frac{Ds}{Dt} = \frac{1}{Re}\frac{\Phi}{\rho h} + \frac{1}{RePr}\frac{1}{\rho h}\nabla^2 h, \tag{15c}$$

where the viscous dissipation term Φ is expressed as

$$\Phi = |\boldsymbol{\omega}|^2 + 2\nabla\mathbf{u} : (\nabla\mathbf{u})^T - \frac{2}{3}\theta^2. \tag{15d}$$

This form is especially convenient for computation because it shares with (15b) the same double contraction of the velocity gradient tensor with its transpose. The continuity equation is

$$\frac{D\rho}{Dt} = -\rho\theta, \tag{15e}$$

and the enthalpy is governed by an equation that is derived from the energy (15c) and continuity (15e) equations,

$$\frac{Dh}{Dt} = -a^2\theta + \frac{\gamma}{Re}\frac{\Phi}{\rho} + \frac{\gamma}{RePr}\frac{1}{\rho}\nabla^2 h, \tag{15f}$$

where γ is the ratio of specific heats (taken to be 1.4) and $a^2 = (\gamma - 1)h$ is the square of the local speed of sound.

Evolution equations for the particle strengths are formed by appropriate treatment of the terms contained in Eqs. (15a)–(15f). Much of the treatment is adapted from incompressible vortex methods, but some new ideas are necessary. Most spatial derivative terms are approximated by PSE, which was originally developed for use in convection–diffusion equations [12] but is extendable to more general contexts. The reader is referred to [14] for further discussion of the treatment; in essence, the differential operator D^β (β is a multi-index denoting the number of derivatives in each direction) is replaced by an integral operator L^ε,

$$D^\beta f(\mathbf{x}) \approx L^\varepsilon f(\mathbf{x}) = \frac{1}{\varepsilon^{|\beta|}} \int_{\mathbb{R}^2} (f(\mathbf{y}) \mp f(\mathbf{x}))\eta_\varepsilon^\beta(\mathbf{x} - \mathbf{y})\, d\mathbf{y}, \tag{16}$$

where η^β is the PSE kernel appropriate for this derivative operator and $\eta_\varepsilon(\mathbf{x}) = \eta(\mathbf{x}/\varepsilon)/\varepsilon^2$. The sign is chosen depending on the order of derivative ($-$ for even derivatives and $+$ for odd) because of the conservation that these choices allow, as will be discussed shortly. The integral is subsequently discretized by a quadrature over the particles:

$$D^\beta f(\mathbf{x}_p) \approx \frac{1}{\varepsilon^{|\beta|}} \sum_q V_q (f_q \mp f_p)\eta_\varepsilon^\beta(\mathbf{x}_p - \mathbf{x}_q). \tag{17}$$

With the appropriate sign chosen, application of (17) in many contexts results in the exact conservation of important global quantities. For example, if the quantity f is governed by a convection–diffusion equation in an unbounded domain, the volume integral of f is time-invariant. When (17) is applied to the Laplacian in this equation, the discrete analog of the volume integral $\sum_p V_p f_p$ is exactly conserved because of the skew symmetry of the terms in the summation and the evenness of the kernel used for Laplacian approximation. Failure to conserve a quantity such as this (e.g., the circulation) can dramatically affect the results of a simulation.

PSE is used for Laplacian terms, as well as for the first derivatives of enthalpy, entropy, dilatation, and vorticity, with separate kernels used for each order of derivative. It should be noted that (17) has been used with $\beta = 2$ (the Laplacian) extensively in vortex methods (see, e.g., [25, 47]) and with $\beta = 1$ (the gradient) in, for example, SPH [34]. Quackenbush *et al.* [41] used the $\beta = 1$ form to compute the gradient of the density, although their formula is not conservative. For the curl terms in (15a), the PSE operator is applied first to the inner

derivatives and then to the outer derivatives only after the products have been evaluated; a similar procedure is followed for analogous divergence terms in (15b). Following this procedure ensures conservation of circulation, which would not be guaranteed if the curl were first applied to each factor in the products and then the derivatives discretized. Note that this explicit treatment of the derivatives in the baroclinic term differs from the "Lagrangian" approach of replacing them with a term involving the material derivative of the velocity (see, e.g., [41]).

Spatial derivatives in the velocity are treated somewhat differently. It is noted that the double contraction term, $\nabla\mathbf{u} : (\nabla\mathbf{u})^T$, resembles the vortex-stretching term in three dimensions, for which Anderson and Greengard [2] have developed a scheme in which the gradient operator is applied to the right-hand side of (8), acting directly on the smoothed velocity kernels. Applying this technique leads to

$$(\nabla\mathbf{u})_p = \sum_q \Gamma_q(t)\nabla\mathbf{K}_\varepsilon(\mathbf{x}_p - \mathbf{x}_q) \times \hat{\mathbf{e}}_3 - \sum_q Q_q(t)\nabla\mathbf{K}_\varepsilon(\mathbf{x}_p - \mathbf{x}_q). \tag{18}$$

The new kernel $\mathbf{R}_\varepsilon = \nabla\mathbf{K}_\varepsilon$ can be written in terms of ζ and q as

$$R_\varepsilon^{ij}(\mathbf{x}) = \frac{\partial K_{\varepsilon,i}}{\partial x_j}(\mathbf{x}) = \left(-\zeta_\varepsilon(\mathbf{x}) + \frac{q(|\mathbf{x}|/\varepsilon)}{\pi|\mathbf{x}|^2}\right)\frac{x_i x_j}{|\mathbf{x}|^2} - \frac{q(|\mathbf{x}|/\varepsilon)}{2\pi|\mathbf{x}|^2}\delta_{ij}.$$

Note that $\lim_{r->0} R_\varepsilon^{ij}(r) = \frac{1}{2}\zeta_\varepsilon(0)\delta_{ij}$. As an example, if the second-order Gaussian function is used, then

$$R_\varepsilon^{ij}(\mathbf{x}) = \frac{1}{\pi|\mathbf{x}|^2}\left[1 - \left(1 + \frac{|\mathbf{x}|^2}{\varepsilon^2}\right)e^{-|\mathbf{x}|^2/\varepsilon^2}\right]\frac{x_i x_j}{|\mathbf{x}|^2} - \frac{1}{2\pi|\mathbf{x}|^2}\left(1 - e^{-|\mathbf{x}|^2/\varepsilon^2}\right)\delta_{ij}.$$

It is certainly appropriate to ask why a uniform treatment is not used for all spatial derivatives; but velocity is not a primary variable, so PSE would not be appropriate for approximating its derivatives. On the other hand, using the velocity derivative treatment for derivatives of primary variables—in other words, applying the derivative operator directly to the blob function—would be analogous to Fishelov's method [17] for incompressible flows. We chose to use PSE because of its conservation properties, however.

Fluid elements expand and contract in compressible flow, and the computational elements will be allowed to do so as well. The particle volumes will thus change according to a restatement of (15e):

$$\frac{dV_p}{dt} = Q_p. \tag{19}$$

This equation ensures that the Jacobian of the flow map is correctly accounted for in the quadrature approximation of volume integrals. Given the initial density of a particle, the density at subsequent times will be calculated through $\rho_p(t) = \rho_p(0)V_p(0)/V_p(t)$. This treatment explicitly ensures that the method conserves mass. It was also employed by Quackenbush *et al.* [41] to account for fluid dilatation by the heat release of combustion.

It is useful to reformulate the equations for the vorticity and dilatation in terms of the integral values of these quantities: the particle circulation Γ_p and the source strength Q_p. This approach, when combined with (19), eliminates the θ term from Eq. (15a) and an analogous term embedded in the double contraction term in Eq. (15b). The final set of

equations for the particle strengths are written in particle-discretized form in the Appendix. Since the method is Lagrangian, particle strengths are functions of time only and the material derivatives in the continuous equations are replaced by ordinary time derivatives. Note that particle strengths are used in place of field quantities in some terms (e.g., $h_p\theta_p$ in (A.5f)), which raises the question of the suitability of such a substitution, especially when the particle locations become disordered. We proceed without proof, though our results will demonstrate that the approach is adequate. These particle evolution equations may be solved simultaneously using a standard time integration scheme, such as the fourth-order Runge–Kutta method. Also needed are initial conditions for the primary variables. Often it may be sufficient to set the initial dilatation and entropy to zero (unless the circumstances of a particular problem require otherwise) and then compute the initial enthalpy from the initial vorticity (or velocity, rather) through a solution of the Poisson problem,

$$\nabla^2 h = -\nabla \mathbf{u}_s : (\nabla \mathbf{u}_s)^T, \tag{20}$$

which are the terms that remain from (15b), less a small viscous term. In many problems these two terms will be in near-perfect balance, though individually much larger than their sum. The ramifications of this behavior will be discussed in Section 4.2. Setting the initial enthalpy in this manner effectively reduces the magnitude of the transient that results from not specifying these initial conditions in an exactly consistent manner. With the initial enthalpy and entropy of a particle specified, the initial particle density can then be computed through

$$\rho_p(0) = [(\gamma - 1)h_p(0)]^{1/(\gamma-1)} \exp\left(-\frac{\gamma}{\gamma - 1} s_p(0)\right), \tag{21}$$

which is the integrated form of the thermodynamic relation $dh = T\,ds + dp/\rho$, combined with the perfect gas relation. Note that these particle strengths initially correspond with the local field values of these quantities, so the use of this relation is justified. The particles are initially located on a uniform Cartesian grid, with $V_p(0) = \Delta x^2$, where Δx is the particle spacing.

3. SPATIAL COMPACTNESS AND DOMAIN TRUNCATION

Extending a vortex particle method from its common use in hydrodynamics to compressible flows introduces the issue of dealing computationally with an unbounded domain. In hydrodynamics, an initially compact vorticity field will only spread as quickly as viscous diffusion allows, and thus the extent of significant levels of vorticity remains limited for moderate times. One of the major motivations for vortex methods is that the particles that carry the vorticity *define* the computational domain, so the methods are efficient and in the absence of solid boundaries all boundary conditions are implicitly accounted for by the Biot–Savart integral. Compressible flows inherently contain radiated components, which are *not* spatially compact. If this radiation is to be accommodated in a numerical method by the exchange of strengths described above, then some means must be provided that allows the outer particles to exchange strength with an infinite region exterior to the particles. Furthermore, the integral for computing the irrotational component of the velocity (the second term of Eq. (3)) must be addressed because its integrand does not confine itself to the particle coverage.

We note that in general it may be possible to retain some measure of the spatial compactness associated with incompressible vortex methods in the extension to compressible flow. It is known that the sources of acoustic waves can be written in terms that are linear in the vorticity and entropy, provided that the stagnation enthalpy, $B = h + \frac{1}{2}|\mathbf{u}|^2$, is taken as the acoustic variable.[2] This shows, then, that the radiated acoustic field may only need to be discretized to a distance after which its amplitude is small enough that its effect on the particle's motion may be neglected. In this external field, the irrotational flow is governed by a linear wave equation. We believe that this feature could be exploited to obviate the need for particle placement in this outer region, but we have not yet developed a systematic procedure to carry it out.

Instead, we propose here a simpler approach, wherein particles are retained to a somewhat larger distance into the acoustic field. At this distance, we merely truncate the computational domain and apply an artificial boundary condition to attempt to allow for only outgoing acoustic waves (i.e., we apply a so-called nonreflecting boundary condition). Nonreflecting boundary conditions remain an active area of research (see reviews [20, 46]). While much progress has been made in developing conditions for linear problems, nonlinear boundary conditions are still in their nascent stage. It will be assumed that, away from the "source" region (usually the region of rotational flow [23]), the particle velocities and fluctuations in the other flow quantities will be much smaller than their characteristic values in the source region. Under such conditions, the vorticity vanishes, products of fluctuations can be neglected, dissipative mechanisms are insignificant except over large distances, and thus the governing equations (15a)–(15f) reduce to the homogeneous linear wave equation,

$$\frac{\partial \theta}{\partial t} = -\nabla^2 h, \tag{22a}$$

$$\frac{\partial h}{\partial t} = -\theta. \tag{22b}$$

Thus, linear boundary conditions are justified.

3.1. *Boundary Condition and Enforcement*

The Engquist–Majda [15] hierarchy of conditions have been successful for a variety of problems. The conditions are developed by forming a series of Padé approximations to the Fourier-transformed pseudodifferential operator representation of Sommerfeld's radiation condition. The conditions are developed for both planar and circular boundaries. For most problems, a circular rather than a rectangular domain is used to avoid complications at the corners. When the term "boundary" is used here, it denotes the farthest extent of particle coverage. The first member of the hierarchy is

$$\left(\frac{\partial f}{\partial t} + \frac{\partial f}{\partial r} + \frac{f}{2r} \right)_{r=R} = 0, \tag{23}$$

where R is the radius of curvature of the boundary and f is any quantity governed by the linear wave equation. A means must be developed for enforcing the condition. We create a

[2] This result is embodied in Howe's acoustic analogy [23], but we refer here primarily to the form developed by Möhring [33], for which the wave operator in the otherwise irrotational and isentropic media takes on a somewhat simplified and self-adjoint form.

new class of boundary particles, which lie on the periphery of the coverage in a "boundary zone," that has a different set of properties from the class of interior particles. The new particles translate as the others do (albeit with a very small motion), but their enthalpy h_p is governed by

$$\frac{dh_p}{dt} = -\left(\frac{\partial h}{\partial r}\right)_p - \frac{(h_p - h_\infty)}{2R_p} \tag{24}$$

instead of (the particle form of) Eq. (15f), where R_p is the radial distance of the particle from the origin. Their dilatation, vorticity (which is zero by assumption), and entropy are held constant. The boundary zone has a depth that depends on the blob radius of the particles; typically only a depth of a few particles is required.

The spatial derivative in (24) is approximated using PSE. However, the technique of approximating the derivative by a full-space integral is inaccurate. A kernel centered at a point near the boundary expects to have information available from an approximately circular (or in three dimensions, spherical) region surrounding the point. If any portion of this region fails to intersect the computational domain, then the subsequent quadrature of the integral will be poor. In these cases a half-space integral is used in lieu of the full-space version (see [14]). The particle-discretized formula is described in the Appendix. If a line (or plane) is drawn through the point in question, parallel to a tangent of the near boundary (see Fig. 1), then the integration proceeds over the "inner" half space Ω_L that contains the domain. The quadrature of the integral will only involve particles located in the half disc shown (or an analogous hemisphere in three dimensions), corresponding to the intersection of the kernel support with the half space. Even this region may have portions that fail to intersect the domain; for a circular boundary the nonintersecting portions will be wedge-shaped. It can be shown, however, that the errors due to such portions scale with their areas, which are small for modestly convex boundaries. The error from such a treatment can be shown to be dominated by the incomplete annihilation of a cylindrical wave by Eq. (23); for a general wave the leading-order error is $O(R^{-5/2})$.

For the second term in Eq. (3), the integration is simply truncated at the boundary of particle coverage. For most flows of interest, the irrotational component is significantly smaller than the solenoidal, and furthermore the dilatation external to the domain is likely to contribute very little to this small irrotational part.

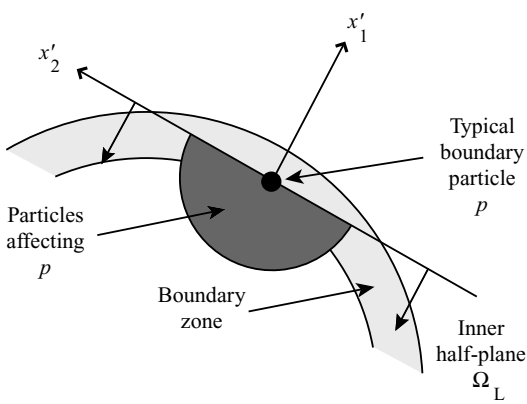

FIG. 1. Schematic of the boundary treatment.

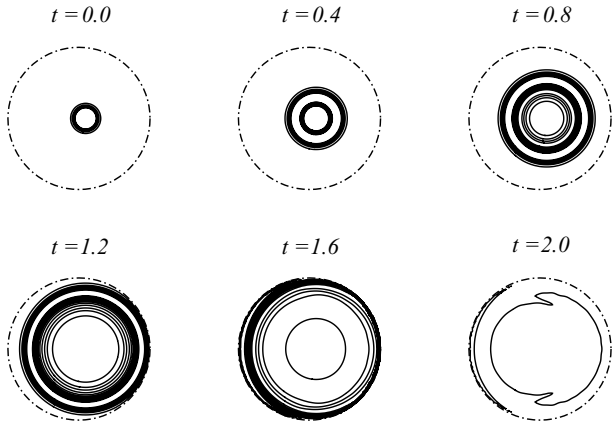

FIG. 2. Results of simulation of enthalpy pulse. The dotted line represents the boundary of the domain.

3.2. *Testing the Condition*

The boundary treatment is tested by simulating a radially symmetric pulse of enthalpy of strength 0.1% of the ambient value, offset slightly from the center of the computational domain. For such a weak perturbation the equations of motion would reduce to the linear wave equation for the enthalpy and dilatation since particle velocities are negligible. Nevertheless we use the full compressible equations in order to test the full method. An eighth-order PSE kernel derived in [14],

$$\eta^{\text{lap}}(\mathbf{x}) = \frac{1}{\pi}\left(40 - 40|\mathbf{x}|^2 + 10|\mathbf{x}|^4 - \frac{2}{3}|\mathbf{x}|^6\right)e^{-|\mathbf{x}|^2},$$

is used in the interior for the Laplacian; surrounding the domain is a boundary zone with a depth of four particles, enforcing Eq. (24) with the second-order one-sided kernel

$$\eta^{L,(1,0)}(\mathbf{x}) = -\frac{4}{\pi}x_1(5 - 2|\mathbf{x}|^2)e^{-|\mathbf{x}|^2}.$$

The initial distribution of enthalpy is Gaussian with a radius $1/10$ the radius of the domain, and 13 particles are distributed across the diameter of the Gaussian. Thus, a total of 13,040 particles are used.

The results of the simulation are depicted in the panels of Fig. 2. As expected the pulse spreads out in a cylindrical wave that travels at the correct speed (the times are given in acoustic units). The wave front reaches the boundary and passes through it with very little reflection—approximately 2% of the incident wave. This reflection can be reduced by making the domain larger, thus decreasing the radius of curvature of the boundary.

4. OTHER ASPECTS

4.1. *Fast Summation*

Lagrangian numerical methods require certain modifications to make them useful for large-scale computation. First of all, the velocity computation in (8) is inherently $O(N^2)$, which would prohibit simulations using more than a few thousand particles. Several fast

summation methods have been developed for reducing this calculation to $O(N \log N)$ or $O(N)$. The fast multipole method (FMM) of Greengard and Rokhlin [21] treats the particles as monopoles and lumps their far-field interactions into interactions between clusters, using formulas that shift the centers of the multipole expansions. A quad-tree structure is used to group nearby particles together and precisely define the concepts of "near neighbors" and "well separated." Near-neighbor interactions are computed directly. The FMM is adapted to the present method by regarding the particles as vortex-source superpositions. It is convenient in two dimensions to describe physical coordinates in terms of the complex variable $z = x_1 + ix_2$. Through this description the particle strength is also complex, $S_p = Q_p - i\Gamma_p$. The velocity field induced on a distant point z by a cluster of m particles centered at z_0 is

$$F(z) = u_1 - iu_2 = \sum_{k=0}^{P} \frac{a_k}{(z - z_0)^{k+1}},$$

where

$$a_k = \frac{1}{2\pi} \sum_{p=1}^{m} S_p (z_p - z_0)^k, \quad k = 0, \ldots, P,$$

and P is the truncated number of terms. The reader is referred to [21] for details of the implementation. The velocity gradient tensor (18) can be computed efficiently with the same method by using the derivative of the complex multipole expansion of the velocity field. Thus, the velocity gradient induced by the same cluster on a point z is

$$F'(z) = \frac{\partial u_1}{\partial x_1} - i \frac{\partial u_2}{\partial x_1} = -\sum_{k=1}^{P+1} \frac{k a_{k-1}}{(z - z_0)^{k+1}},$$

and the Cauchy–Riemann equations can be used to get the other components of the tensor. Figure 3 depicts the CPU time required to complete a single time step on a 500-MHz Compaq Alpha XP1000 workstation. The number of particles was varied from about 38,000 to about 277,000. The CPU time scales as $O(N)$ as predicted.

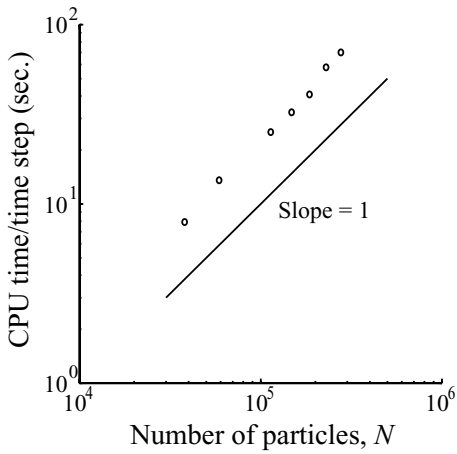

FIG. 3. CPU time for several different particle populations.

It is important to note that despite the description in terms of complex coordinates, the FMM is not limited to two-dimensional flows. The method has been extended to three-dimensional problems using the same basis of the multipole expansion, albeit with different formulas that employ spherical harmonics and an oct-tree structure in lieu of the quad-tree. Formulas are given in [16] and the appendix of [9] provides a useful discussion.

The FMM was originally designed for singular particles. Since the width of such particles is zero, only one particle per box is required at the finest level of the quad-tree. A particle thus only directly communicates with eight neighbors. However, the blobs used in the present method have a finite size. For the multipole expansion of a cluster to be valid at a given point, the members of that cluster should be indistinguishable from the singularities that they are designed to resemble. This restriction necessitates larger boxes at the finest level to ensure only direct interactions between particles that appear as blobs to one another. As the number of particles is changed, the quad-tree must be adjusted to keep the number of particles per box, N_{box}, within a certain range: if N_{box} is too small, then the near-neighbor list is too small and important direct interactions are neglected; if N_{box} is too big, then the computation time is dominated by unnecessary direct near-neighbor interactions.

The hierarchy of boxes used in the FMM provides a natural framework for efficiently computing other pieces of the method. The PSE summations are truncated to include only interactions between particles in near-neighbor boxes. This treatment is consistent with the defining property of near neighbors, that particles only resemble blobs inside the near-neighbor region, because PSE kernels are close cousins with the blob function and decay with nearly the same rapidity. Although high-order-accurate PSE kernels certainly have larger support than lower order ones, their support is still confined to the near-neighbor region, and interactions beyond this region are neglected.

4.2. *Remeshing*

A second necessary modification of the basic method—remeshing—arises because of the topology of the flow. The flow will often contain regions of high accumulated strain where fluid elements have been stretched. Such behavior is reflected in those regions becoming sparsely populated with computational elements, thus violating the convergence requirement of vortex methods that the blobs overlap. Particles must periodically be redistributed to prevent such accumulation. It is desirable to conserve global flow quantities such as the mass, circulation, and angular impulse in this process. Interpolation of this type was addressed by Schoenberg [44] and has proved an essential part of SPH [34] and vortex particle methods [9].

Extra care must be taken when interpolating in the present method because of the sensitivity of the acoustic field to even the smallest errors. This occurs because the first and second terms on the right-hand side of (15b) are in many cases in near-perfect balance. The slight imbalance, however, is crucial to the sound generation process (see, for example, the singular perturbation analysis of [10]) and thus extremely important to accurate computation. Through trial and error, we have found that interpolation can degrade the smoothness of the enthalpy and introduce an error that is subsequently amplified by PSE. This error can overwhelm (15b) unless the interpolation error is substantially reduced. To ensure stability in the DVPM, many common interpolation kernels, such as the M_4' kernel of [34], carry stringent requirements of particle spacing and remeshing frequency. For instance, using the M_4'

kernel in the corotating vortex problem discussed below, we found that stability demands that 21 particles be placed across the diameter of each vortex and that the particles be remeshed every step. We discovered that a higher order interpolation with some degree of smoothing as described below, using kernels of Gaussian type, is much less restrictive, but at the cost of not exactly conserving the global quantities (although the departure is only slight). For the same problem, the sixth-order kernel derived presently requires only 13 particles and remeshing only every 10 steps to remain stable. Further refinement reduces the smoothing, thus making it necessary to remesh more frequently. In practice we remesh every one or two steps. This frequency was chosen by trial and error; it proves to be quite difficult to develop a general rule by which to measure acceptable grid distortion, as ultimately the decision must be problem-specific.

It should be pointed out that the need for smoothing in remeshing is not new to vortex methods. Cottet [8] found in his incompressible simulations of decaying two-dimensional turbulence that a slightly dissipative remeshing scheme was necessary to prevent noise build-up from preventing the self-organizing of small-scale vorticity into large coherent eddies.

The interpolation can be expressed in a continuous sense as

$$\tilde{f}(\mathbf{x}) = \int W_\sigma(\mathbf{x}-\mathbf{y}) f(\mathbf{y})\, d\mathbf{y}, \tag{25}$$

where $\tilde{f}(\mathbf{x})$ is the new value of the function at position $\mathbf{x}$, and $W_\sigma(\mathbf{x}) = W(\mathbf{x}/\sigma)/\sigma^2$ is the interpolation kernel scaled by the interpolation radius σ, alternatively regarded as the degree of smoothing in the interpolation. Ideally, $\tilde{f}(\mathbf{x}) = f(\mathbf{x})$. However, we settle for $\tilde{f}(\mathbf{x}) = f(\mathbf{x}) + O(\sigma^r)$, where r is the order of accuracy of the interpolation kernel. The form of Eq. (25) is similar to the integral operator of PSE. Using the same Taylor expansion approach here as in the PSE derivation of [14], we develop the relation

$$f(\mathbf{x}) = \frac{1}{M_{(0,0)}}\left[\int W_\sigma(\mathbf{x}-\mathbf{y}) f(\mathbf{y})\, d\mathbf{y} - \sum_{j=1}^{\infty}\sum_{k=0}^{j} \frac{(-\sigma)^j}{j!} D^{(k,j-k)} f(\mathbf{x}) M_{(k,j-k)}\right],$$

where the operator $D^{(\alpha_1,\alpha_2)}$ is defined as $D^\alpha = D^{(\alpha_1,\alpha_2)} = \frac{\partial^{|\alpha|}}{\partial x_1^{\alpha_1}\partial x_2^{\alpha_2}}$, where $|\alpha| \equiv \alpha_1 + \alpha_2$, and the moments M_α are defined as in [14],

$$M_\alpha = \int_{-\infty}^{\infty}\int_{-\infty}^{\infty} y_1^{\alpha_1} y_2^{\alpha_2} W(\mathbf{y})\, dy_1\, dy_2. \tag{26}$$

The conditions on these moments are given by

$$M_\alpha = \begin{cases} 1, & \alpha = (0,0), \\ 0, & |\alpha| \in [1, r-1], \end{cases} \tag{27a}$$

as well as

$$\int_{-\infty}^{\infty}\int_{-\infty}^{\infty} |\mathbf{y}|^r |W(\mathbf{y})|\, dy_1\, dy_2 < \infty. \tag{27b}$$

Note that these conditions are *identical* to those imposed on the blob function. We have chosen to use a template that is the product of two one-dimensional polynomials and a Gaussian,

$$W(x_1, x_2) = \frac{1}{\pi}\left(\sum_{j=0}^{m} \gamma_j x_1^{2j}\right)\left(\sum_{j=0}^{m} \gamma_j x_2^{2j}\right) e^{-(x_1^2+x_2^2)}, \tag{28}$$

where $m = r/2 - 1$. Kernels of this family are more smooth than the M_4' kernel—the M_4' kernel does not have continuous derivatives at distances of one and two particle spacings away—and thus have better stability properties. Through experience we have found that a sixth-order kernel works well for interpolation:

$$W(x_1, x_2) = \frac{1}{\pi}\left(\frac{15}{8} - \frac{5x_1^2}{2} + \frac{x_1^4}{2}\right)\left(\frac{15}{8} - \frac{5x_2^2}{2} + \frac{x_2^4}{2}\right) e^{-(x_1^2+x_2^2)}.$$

The particle vorticity, dilatation, density, and entropy are interpolated using the discrete analog of (25),

$$\tilde{f}_p = \sum_q W_\sigma(\tilde{\mathbf{x}}_p - \mathbf{x}_q) V_q f_q, \tag{29}$$

where $\sigma = 1.7\Delta x$, $\{V_p\}$ are the old particle volumes, and $\{\tilde{\mathbf{x}}_p\}$ are the new particle positions.

The integral moment conditions on W ensure the invariance of the corresponding integral moments of the interpolated quantities during remeshing, some of which are governed by physical conservation laws in two-dimensional flows. For instance, the zeroth moments of density and vorticity—the mass and circulation, respectively—are conserved in such flows. It is thus important that these quantities not change appreciably during remeshing. By enforcing the conditions on the integral moments of W, the corresponding discrete moment conditions (e.g., $\sum_p W(\mathbf{x}_p) = 1$) are nearly satisfied.

5. RESULTS AND DISCUSSION

5.1. *Corotating Vortex Pair*

The method was first applied to a pair of identical vortices in a compressible medium. As the vortices orbit each other they generate sound at a frequency of twice their rotation rate. The problem has been explored by several researchers (e.g., Müller and Obermeier [38], Yates [48]) and recently simulated by Mitchell, Lele, and Moin [31] using a compact finite-difference method on a stretched grid. The initial configuration of the vortices is depicted in Fig. 4. All quantities are scaled by the initial half spacing between the vortices R and the ambient speed of sound a_∞. For comparison with Mitchell *et al.* [31], each vortex is Gaussian-distributed according to

$$\omega = \frac{1.25\Gamma_0}{\pi r_0^2} e^{-1.25r^2/r_0^2},$$

where the circulation and radius of each vortex are $\Gamma_0 = -2\pi(0.7)^{-1} M_0 r_0$ and $r_0 = 0.15$, respectively. The circulation Reynolds number $Re \equiv |\Gamma_0|/\nu$ is 7500, the vortex Mach number $M_0 \equiv U_0/a_\infty$ (where U_0 is the maximum azimuthal velocity of a single Gaussian vortex)

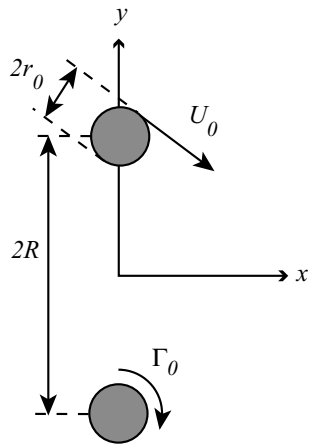

FIG. 4. Initial configuration of vortex pair.

is 0.56, and the Prandtl number is 0.7. With these flow parameters, the initial rotation time is $\tau = 105$ and the wavelength of sound is $\lambda = 52.5$. Such a large separation in the acoustic and flow length scales qualifies the vortices as a compact source, which makes efficient resolution of the problem difficult. Instead of attempting to capture both the near and far fields simultaneously, the present investigation focused on the near-field dynamics only. The method is capable of computing both, but without particles of variable size it cannot compute both regions practically.

Initially, the flow is taken as homentropic and dilatation-free. The initial enthalpy is deduced from a solution of the Poisson equation (20), which is solved with the same Green's function approach used to invert the potential equations (1). The particles are distributed on a Cartesian grid inside a circular domain of radius R_Ω with N_{core} particles laid across the diameter of each vortex; a boundary zone with a depth of four particles surrounds the domain. The particles are remapped to the same Cartesian grid every n_{rm} time steps. A fourth-order Runge–Kutta scheme is used for time advancement with a time-step size of $\Delta t = 0.009$. The blob radius and particle spacing are related by $\varepsilon = \Delta x^{0.85}$. All of the kernels used in the interior are eighth-order accurate, except for the one-sided boundary kernel, which is second-order accurate.

Blob function:	$\zeta(\mathbf{x}) = \frac{1}{\pi}\left(4 - 6\lvert\mathbf{x}\rvert^2 + 2\lvert\mathbf{x}\rvert^4 - \frac{1}{6}\lvert\mathbf{x}\rvert^6\right)e^{-\lvert\mathbf{x}\rvert^2}$
Laplacian:	$\eta(\mathbf{x}) = \frac{1}{\pi}\left(40 - 40\lvert\mathbf{x}\rvert^2 + 10\lvert\mathbf{x}\rvert^4 - \frac{2}{3}\lvert\mathbf{x}\rvert^6\right)e^{-\lvert\mathbf{x}\rvert^2}$
First derivative wrt x_i:	$\eta(\mathbf{x}) = \frac{x_i}{\pi}\left(-20 + 20\lvert\mathbf{x}\rvert^2 - 5\lvert\mathbf{x}\rvert^4 + \frac{1}{3}\lvert\mathbf{x}\rvert^6\right)e^{-\lvert\mathbf{x}\rvert^2}$
Bndry first deriv. wrt x_i:	$\eta^L(\mathbf{x}) = \frac{x_i}{\pi}(-20 + 8\lvert\mathbf{x}\rvert^2)e^{-\lvert\mathbf{x}\rvert^2}$

To verify that the method converges as the particle coverage is refined, we computed the problem on a domain of radius $R_\Omega = 2.5$ and let $N_{\text{core}} = 10$, 13, 20, and 40. The resulting dilatation field at a point $(x, y) = (0, 1.2)$, shown in Fig. 5, converges as the particles are more densely packed. With 13 particles across each vortex core, the results are sufficiently converged.

The results of the vorticity and dilatation fields from a computation with $N_{\text{core}} = 13$, $R_\Omega = 4$ (corresponding to about 83, 500 particles), and $n_{rm} = 2$ are depicted in the series of

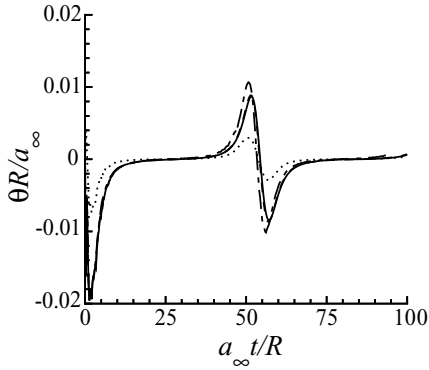

FIG. 5. Dilatation at $(x, y) = (0, 1.2)$. $N_{\text{core}} = 10$, · · · · · ·; 13, —·—·—; 20, – – –; 40, —.

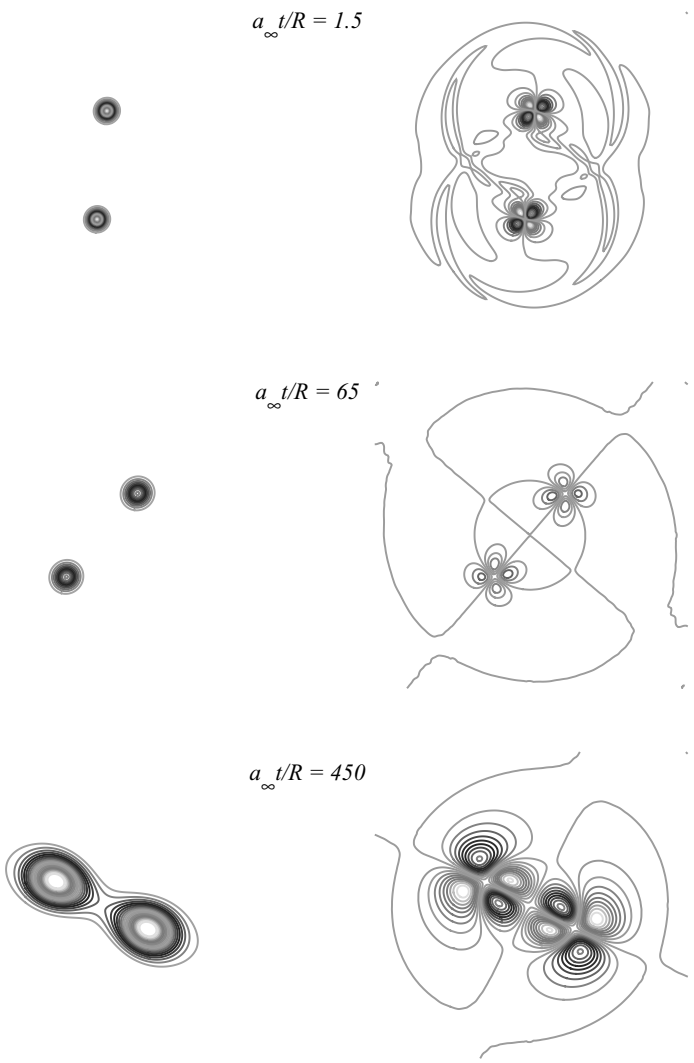

FIG. 6. Vorticity (left) and dilatation (right) in corotating vortex pair.

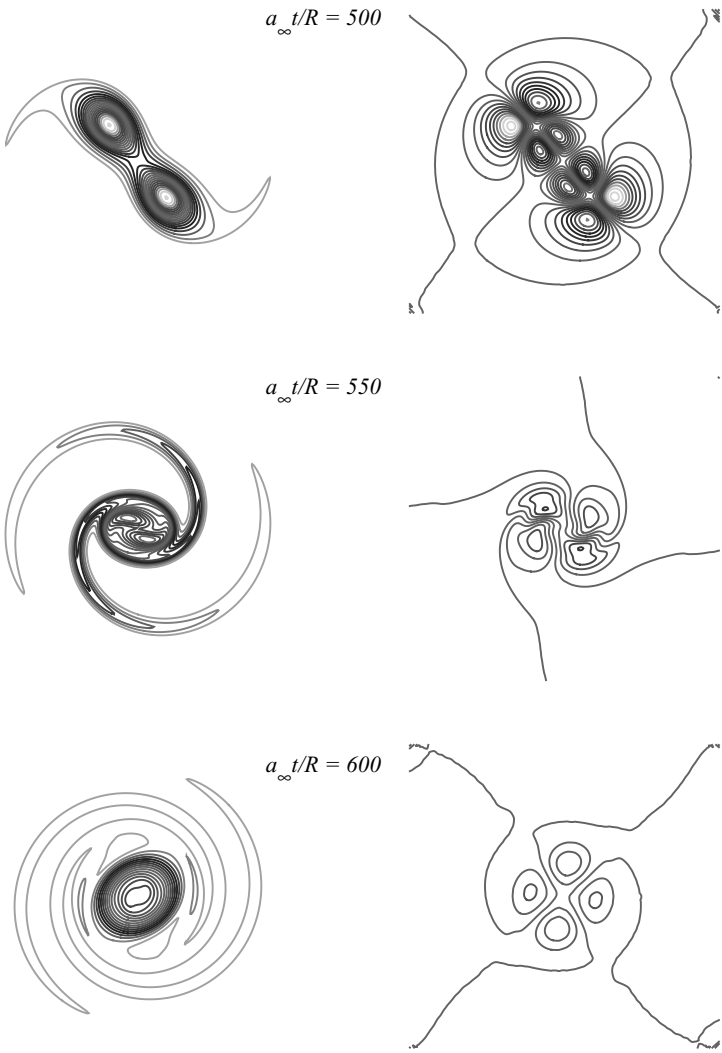

FIG. 6—*Continued*

panels of Fig. 6. Note that both fields are scaled by U_0 and R for these figures. For the dilatation panels, dark contours denote positive values and light denote negative. The contour levels are as follows: for the first two time levels, the vorticity levels are in the range $[-23, -1]$ in increments of $\Delta\omega = 1$ and the dilatation levels are in $[-0.06, 0.06]$ in increments of $\Delta\theta = 0.006$; the remaining four time levels have vorticity contours in $[-2, -0.05]$ in increments of $\Delta\omega = 0.103$ and dilatation contours in $[-0.005, 0.005]$ in increments of $\Delta\theta = 0.0005$. The first row of panels shows the fields soon after the initialization. An acoustic transient is emitted from each core as the dilatation settles to the correct value; the transient is not strong and exits the domain without significant reflection. A quadrupole structure is observed in the dilatation in the next row of panels. The same structure was observed by Mitchell *et al.* [31] as well as by Yates [48] in his Bernoulli enthalpy, a quantity that is closely related to the dilatation. The configurations of both fields persist for several rotations, though both quantities are diffused by viscosity over this duration, as observed in

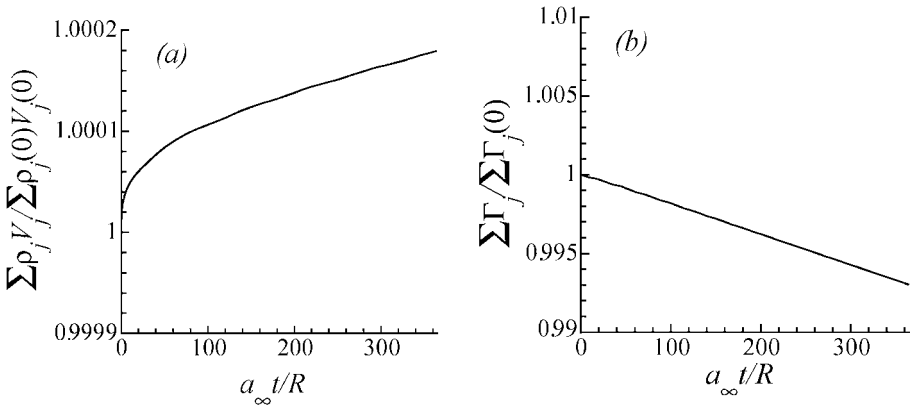

FIG. 7. Histories of the (a) total mass and (b) total circulation of the particles.

the third set of panels (in which the contour levels have been adjusted for better resolution of the diffused magnitudes). After approximately four rotations the continual effects of viscosity and compressibility force the cores to merge, depicted in the final three rows of panels. The resulting dilatation field is a much weaker quadrupole centered at the core of the new elliptical vortex. Further computation, not shown, reveals the axisymmetrization of the core and thus the disappearance of the dilatation.

In viscous vortex methods, an important parameter is the grid Reynolds number, which can be defined as $Re_h \equiv |\omega|\Delta x^2/\nu$. When $Re_h = O(1)$, the smallest length scales in a viscous flow will be well resolved. With $N_{\text{core}} = 13$, the particle spacing is $\Delta x = 0.025$, and thus initially $Re_{h,\max} \approx 83$. This value is significantly higher than the recommended value of 1. However, computing the same flow with $N_{\text{core}} = 40$, corresponding to $Re_{h,\max} \approx 7$, did not introduce any new structures. The fine structures in the flow do not appear until later times, as depicted in Fig. 6, when the maximum vorticity has decreased substantially and $Re_{h,\max} = O(1)$.

The conservation properties of the DVPM are demonstrated by plotting the total mass and circulation in the domain versus time in Fig. 7. The total mass of the particles rises by less than 0.02% and the total circulation decays by less than 1%. The deviations are due wholly to the fact that the interpolation kernel we have chosen does not exactly conserve the zeroth moment of interpolated quantities, as discussed above. The change in circulation is more dramatic than the change in mass: since only the difference in a particle's density from the ambient value is interpolated, and $|\Delta\rho|/\rho_\infty$ is small, the mass is less affected by the interpolation error. Neither quantity changes enough to significantly affect the results.

5.1.1. Kirchhoff surface. Provided that the computational domain extends into the acoustic region, the entire far-field solution can be deduced from the limited acoustic information available from the near-field simulation through the use of a Kirchhoff surface. For a field quantity f governed by the linear, homogeneous wave equation in Ω_e, the Kirchhoff equation expresses its solution in this domain in terms of its boundary and initial values.

In two dimensions, provided that the initial values of f and its derivative are zero in the exterior domain and on its interior boundary $\partial\Omega_e$, the solution $f(\mathbf{x}, t)$ in Ω_e can be

expressed as

$$f(\mathbf{x},t)=\frac{1}{2\pi}\int_{\partial\Omega_e}\int_0^{t^*}\left[\left(\frac{\partial f}{\partial\tau}+\frac{f(\mathbf{y},\tau)}{t-\tau+|\mathbf{x}-\mathbf{y}|}\right)(\hat{\mathbf{e}}_R\cdot\mathbf{n}_y)-\frac{\partial f}{\partial n_y}(\mathbf{y},\tau)\right]\times\frac{d\tau\,dS(\mathbf{y})}{\sqrt{(t-\tau)^2-|\mathbf{x}-\mathbf{y}|^2}}. \tag{30}$$

The time integral is integrated to the retarded time $t^*=t-|\mathbf{x}-\mathbf{y}|$. The vector $\hat{\mathbf{e}}_R$ is the unit vector from the surface position $\mathbf{y}$ in the direction of the observation point $\mathbf{x}$; $\mathbf{n}_y$ is the *inward* normal at $\mathbf{y}$ (or outward from the interior region).

The choice of the variable f in part determines how far one must go from the nonlinear source region to find the acoustic region. If, for example, the enthalpy is chosen, then the region in which this variable is entirely acoustic is apparently quite distant from the source. Outside of the vortical region, the enthalpy obeys Bernoulli's equation: $h=h_\infty-\frac{1}{2}|\mathbf{u}|^2-\frac{\partial\chi}{\partial t}$, where χ is the scalar potential consistent with the velocity induced by the vorticity. An asymptotic matching of the near- and far-field solutions reveals that, while an expansion of $\frac{\partial\chi}{\partial t}$ matches the outer solution term by term, the $\frac{1}{2}|\mathbf{u}|^2$ term has no counterpart in the far field yet persists to large distances because it decays as $1/r^2$. A more appropriate acoustic variable—consistent with the discussion in Section 3—is the stagnation enthalpy $B=h+\frac{1}{2}|\mathbf{u}|^2$. In the irrotational region, $B=B_\infty-\frac{\partial\chi}{\partial t}$, so it satisfies the acoustic equations just outside of the vortical region; in the far field, B and h are equal.

The integrals of Eq. (30) are discretized in space and time. A circular Kirchhoff surface of radius 3.5 surrounds the vortical region; at this radius it is sufficiently removed from the edge of the computational domain to avoid corruption from the boundary treatment. The stagnation enthalpy of each particle is computed from the results of the DVPM simulation and the particle data are interpolated onto the surface control points. The time derivative is computed from backward differencing, and the normal derivative is from a PSE calculation.

The resulting pressure fluctuations—equal to the stagnation enthalpy after nondimensionalizing—observed at one half-wavelength from the origin (on the y-axis) are depicted in Fig. 8. Note that because of the symmetry of the problem each rotation of the vortices

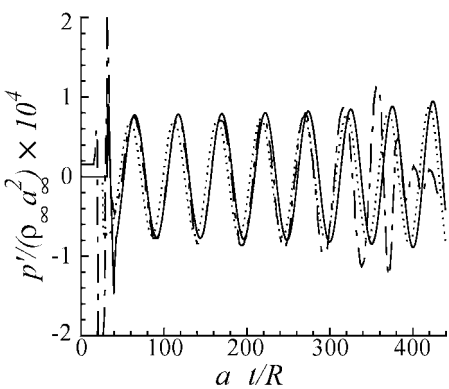

FIG. 8. Pressure fluctuations observed at $(x, y)=(0, \frac{1}{2}\lambda)$. Mitchell *et al.*, –·–; DVPM and Kirchhoff surface at $R_s=3.5$, —; DVPM and Möhring analogy, · · · · · ·.

corresponds to two wavelengths of sound. The magnitude and phase of the pressure agree quite well for the first two rotations. The large spike in Mitchell's data at the outset is due to the acoustic transient. Such a spike is not exhibited in the present results because the initial transient period is ignored in the Kirchhoff calculation. After a little more than three rotations the vortices in Mitchell's simulation merge, reflected by a small rise and then quick decay of the pressure. Merger in the present simulation, though, is delayed by an extra one-and-a-half rotations. As demonstrated by Melander *et al.* [30], incompressible vortices which are initially separated by more than the critical distance for convective merger persist in a "metastable" state for a duration dependent upon a viscous time scale. The vortices eventually undergo convective merger, but the time at which this begins may be quite sensitive to small perturbations. Thus, it is not surprising that merger occurs later in our simulation.

5.1.2. Möhring analogy. The compactness of the vortical flow region allows the use of one of several acoustic analogies for computing the far-field sound. The analogy proposed by Möhring [32] and validated for this problem by Mitchell *et al.* [31] requires only the third time derivative of the second moments of vorticity to calculate the pressure at points outside of the source region. The expression for the pressure, adapted to two-dimensional flow [31], is

$$\frac{p - p_\infty}{\rho_\infty a_\infty^2} = \frac{1}{8\pi} \int_0^\infty \left[\frac{d^3 Q_1}{dt^3}(t^*) \cos(2\theta) + \frac{d^3 Q_2}{dt^3}(t^*) \sin(2\theta) \right] d\xi, \tag{31}$$

where $t^* = t - (r/a_\infty)\cosh(\xi)$ is a modified retarded time that reflects the dependence of two-dimensional sound waves on all events prior to $t - r/a_\infty$. The expressions for Q_1 and Q_2 are

$$Q_1 \equiv 2 \int\int xy\omega \, dx \, dy, \quad Q_2 \equiv \int\int (y^2 - x^2)\omega \, dx \, dy. \tag{32}$$

Clearly Q_1 and Q_2 are available from an incompressible simulation of this flow using existing methods; the far-field analysis considered here is only for completeness. The results agree favorably with the Kirchhoff results and those of Mitchell *et al.* [31], as depicted in Fig. 8.

5.1.3. Noncompact flow field. The difficult task of capturing both the near-field dynamics and the far-field acoustics is alleviated when the acoustic wavelength is not large compared to the extent of the vortical region. As a further demonstration of the capabilities of the DVPM, the same problem was simulated with larger vortex cores, $r_0 = 0.45$, which corresponds to a wavelength of $\lambda = 17.5$. Larger cores permit a larger region to be covered by particles. Using the same number of particles as in the previous simulation, the computational domain was enlarged to a radius $R_\Omega = 12$. The resulting dilatation field at $t = 81$ is depicted in Fig. 9, with the contour levels saturated to elucidate the outer dilatation. At the time shown, the vortices are merging. It is interesting to note that Mitchell *et al.* [31] did not observe merger after five full rotations, or 175 units of time, using vortices of the same size but with a much larger Reynolds number. The counter-clockwise tilting of the dilatation structure in the outer regions is due to the phase lag of compressibility.

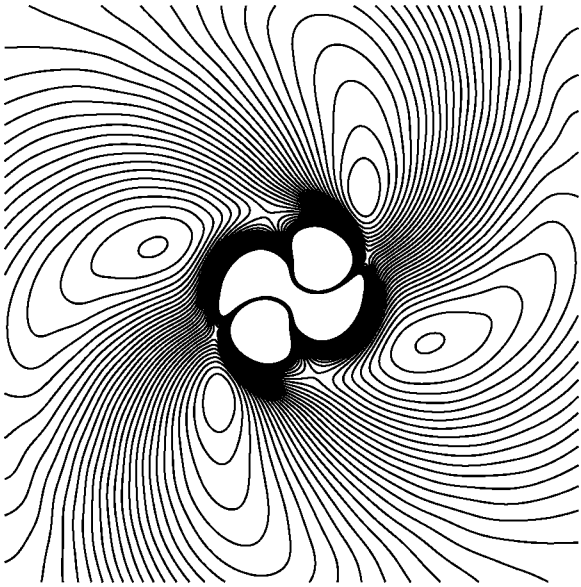

FIG. 9. Dilatation field at $a_\infty t/R = 81$ for a noncompact vortex pair. The contours are saturated for clarity of the outer dilatation field.

5.2. *Baroclinic Generation of Vorticity*

The previous example demonstrated the ability of the DVPM to capture the near-field dilatation, although the effect of compressibility on the overall flow was quite weak. The following problem exhibits the capabilities of the method when gradients in thermodynamic quantities are integral to the flow. A planar enthalpy wave travels through an entropy inhomogeneity, or spot, creating vorticity through the baroclinic source term. The resulting vorticity field can be predicted analytically if the wave and spot are sufficiently weak in magnitude. Suppose that the enthalpy has the initial distribution

$$h(x_1, x_2, 0) = h_R + \frac{\Delta h}{2}\left[\tanh\left(\frac{x_1 - x_h}{\Delta x_h}\right) - 1\right],$$

and the entropy has

$$s(x_1, x_2, 0) = s_\infty + \Delta s \exp\left[-\frac{(x_1 - x_s)^2 + x_2^2}{\sigma_s^2}\right],$$

where $\Delta h > 0$ and $\Delta s < 0$. If both of these quantities are small relative to their ambient values, and the entropy is smaller than the enthalpy $|\Delta s|/|\Delta h| \ll 1$, then the vorticity approximately satisfies

$$\frac{\partial \omega}{\partial t} = \nabla h \times \nabla s,$$

the enthalpy obeys the homogeneous linear wave equation, and the entropy is steady. The enthalpy wave travels across the spot at a speed much faster than the velocity induced by

the resulting counter-rotating vortex pair, whose distribution is given by

$$\omega(x_1, x_2, t) = \Delta s \Delta h \left[\tanh\left(\frac{x_1 - x_h - t}{\Delta x_h} \right) - \tanh\left(\frac{x_1 - x_h}{\Delta x_h} \right) \right] (x_2 - x_s) e^{-(x_1 - x_s)^2 - x_2^2},$$

where the variables have been scaled by a_∞ and σ_s. We used values of $\Delta h = 0.01$, $\Delta s = -0.0001$, $\Delta x_h = 0.5$, $x_h = -3.5$, and $x_s = 0$. For the numerical solution we used particles on a square grid of side length $10\sigma_s$, with 25 particles across the entropy spot and a boundary zone at the right (outgoing) boundary with a 4-particle depth, corresponding to a total of 14,637 particles. A time step size of $a_\infty \Delta t / \sigma_s = 0.01$ was used. The vorticity that results from the simulation is shown in Figs. 10 and 11. The agreement is very good.

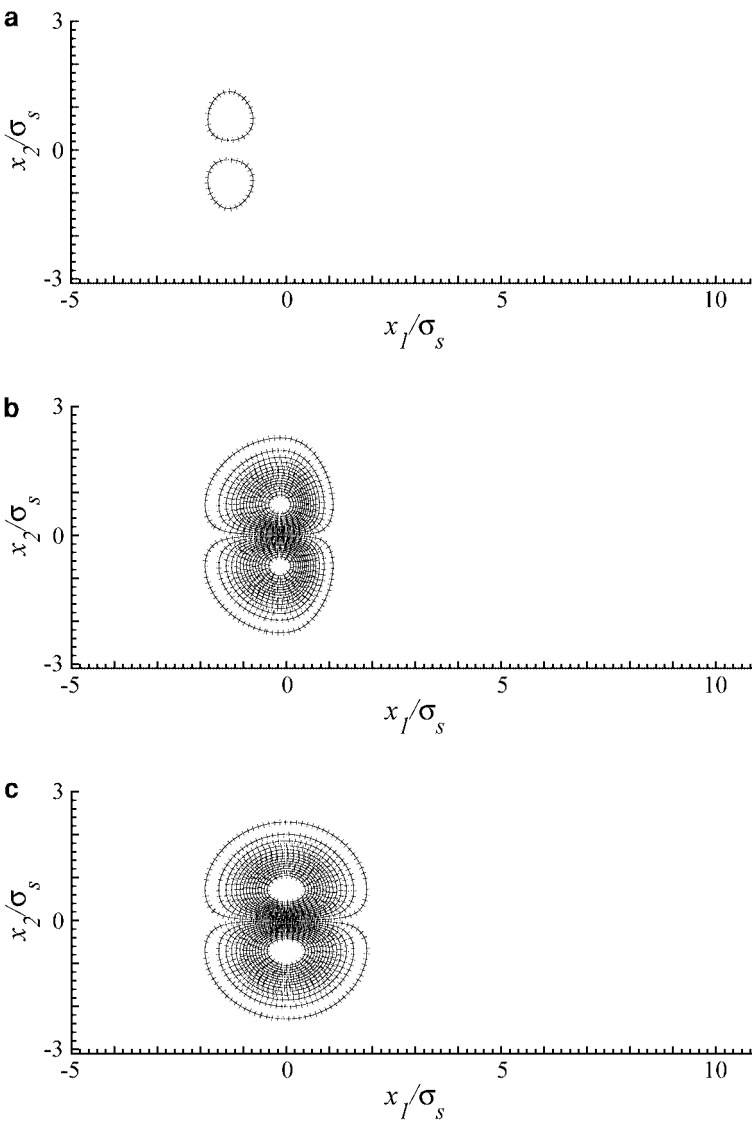

FIG. 10. Vorticity generated by enthalpy wave/entropy spot interaction at (a) $a_R t/\sigma_s = 0.2$, (b) 0.4, and (c) 0.6. DVPM, —; exact, – – –.

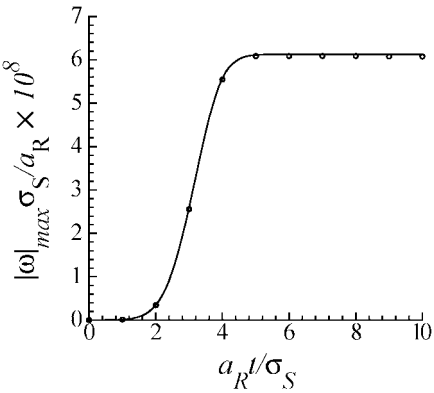

FIG. 11. Maximum vorticity generated by enthalpy wave/entropy spot interaction as a function of time. DVPM, ○; exact, —.

6. CONCLUSION

A vortex particle method for unsteady two-dimensional compressible flow has been developed. This method is the first Lagrangian method for simulation of the full compressible equations of motion, though its construction has relied on existing techniques where possible. By using particles that are able to change volume and that carry vorticity, dilatation, enthalpy, entropy, and density, the method satisfies the equations of motion. A scheme for enforcing a nonreflecting boundary condition has also been introduced and successfully implemented. The fast multipole method has been adapted to compressible particles for more efficient implementation. The new vortex method has been applied to corotating vortices in a compressible medium and to the baroclinic generation of vorticity, and the results agree well with those of previous work or analytical prediction.

Though some previous methods included treatments of compressibility effects (e.g., [18, 41]) that were useful to the present development, those methods relied on simplifying assumptions that would preclude direct simulation of the acoustic field. Because of the small relative magnitude of the acoustic field, our method requires more delicate application of techniques that have proven robust for incompressible vortex methods, for instance computation of derivatives using PSE (which must now suppress dispersion of waves) and interpolation during remeshing (which must preserve smoothness in the interpolated quantities). This subtle balance comes as no suprise as workers in computational aeroacoustics have long been cognizant of the need for high-order methods (e.g., Lele [28]).

We believe this method shows promise, but further developments are necessary to solve problems of larger scale. A more "efficient" definition of the particles—for instance, a division of the particles into those which are active and those which are passive in the velocity induction—is currently being explored, possibly using domain decomposition techniques. Such a division would permit simulations with two different time steps when the time scales of physical phenomena in the flow are distinct. Along the same lines, an implementation of the method with variably sized particles, which would allow more efficient resolution of flows with disparate length scales, is under development. Such an extension would make simultaneous solution of the near and acoustic fields practical. The boundary treatment proposed here is sufficient for absorbing incident acoustic waves, but as discussed in Section 3, it does not fully exploit the decomposition of the velocity at the heart of the method. A more

natural scheme is currently being developed. Finally, using existing techniques for computing vortex stretching, we believe that the method is readily extendable to three-dimensional flows.

APPENDIX: 2-D PARTICLE EVOLUTION EQUATIONS

Here we apply the treatments described in Sections 2 and 3.1 to the equations of motion in two space dimensions and then write the particle evolution equations in their entirety. To write them in their most "compact" forms, we define certain shorthand symbols. In PSE, the difference of strengths between two particles is commonly used:

$$\Delta f_{qp} = f_q - f_p. \tag{A.1}$$

Many different kernels are used in the method. For instance, in the particle velocities, the regularized kernel is written as

$$\mathbf{K}_{\varepsilon,pq} = \mathbf{K}_\varepsilon(\mathbf{x}_p - \mathbf{x}_q), \tag{A.2}$$

the regularized velocity gradient kernel is shortened to

$$\left(R_\varepsilon^{ij}\right)_{pq} = \frac{\partial K_{\varepsilon,i}}{\partial x_j}(\mathbf{x}_p - \mathbf{x}_q), \tag{A.3}$$

and the PSE kernel is expressed as

$$\eta_{\varepsilon,pq}^{(\alpha_1,\alpha_2)} = \eta_\varepsilon^{(\alpha_1,\alpha_2)}(\mathbf{x}_p - \mathbf{x}_q), \tag{A.4}$$

where the superscript indicates the α_1th derivative in the x_1 direction and the α_2th derivative in the x_2 direction. Using this notation, the full equations are

$$\frac{d\mathbf{x}_p}{dt} = \sum_q \Gamma_q \mathbf{K}_{\varepsilon,pq} \times \hat{\mathbf{e}}_3 - \sum_q Q_q \mathbf{K}_{\varepsilon,pq}, \tag{A.5a}$$

$$\begin{aligned}
\frac{d\Gamma_p}{dt} = {} & \frac{V_p}{\varepsilon^2} \sum_{q,r} V_q V_r \left(h_q(s_r + s_q)\eta_{\varepsilon,qr}^{(0,1)} + h_p(s_r + s_p)\eta_{\varepsilon,pr}^{(0,1)}\right)\eta_{\varepsilon,pq}^{(1,0)} \\
& - \frac{V_p}{\varepsilon^2} \sum_{q,r} V_q V_r \left(h_q(s_r + s_q)\eta_{\varepsilon,qr}^{(1,0)} + h_p(s_r + s_p)\eta_{\varepsilon,pr}^{(1,0)}\right)\eta_{\varepsilon,pq}^{(0,1)} \\
& + \frac{1}{Re}\frac{1}{\varepsilon^2} \sum_{q,r} \left\{ \frac{V_p}{\rho_q}\left[\frac{4}{3}(V_q Q_r + V_r Q_q)\eta_{\varepsilon,qr}^{(0,1)} + (V_q \Gamma_r + V_r \Gamma_q)\eta_{\varepsilon,qr}^{(1,0)}\right] \right. \\
& \left. + \frac{V_q}{\rho_p}\left[\frac{4}{3}(V_p Q_r + V_r Q_p)\eta_{\varepsilon,pr}^{(0,1)} + (V_p \Gamma_r + V_r \Gamma_p)\eta_{\varepsilon,pr}^{(1,0)}\right] \right\} \eta_{\varepsilon,pq}^{(1,0)} \\
& - \frac{1}{Re}\frac{1}{\varepsilon^2} \sum_{q,r} \left\{ \frac{V_p}{\rho_q}\left[\frac{4}{3}(V_q Q_r + V_r Q_q)\eta_{\varepsilon,qr}^{(1,0)} - (V_q \Gamma_r + V_r \Gamma_q)\eta_{\varepsilon,qr}^{(0,1)}\right] \right. \\
& \left. + \frac{V_q}{\rho_p}\left[\frac{4}{3}(V_p Q_r + V_r Q_p)\eta_{\varepsilon,pr}^{(1,0)} - (V_p \Gamma_r + V_r \Gamma_p)\eta_{\varepsilon,pr}^{(0,1)}\right] \right\} \eta_{\varepsilon,pq}^{(0,1)},
\end{aligned} \tag{A.5b}$$

$$\begin{aligned}
\frac{dQ_p}{dt} = {} & 2V_p \left\{ \sum_{q,r} \left[\Gamma_q \left(R_\varepsilon^{21}\right)_{pq} - Q_q \left(R_\varepsilon^{11}\right)_{pq}\right]\left[-\Gamma_r \left(R_\varepsilon^{12}\right)_{pr} - Q_r \left(R_\varepsilon^{22}\right)_{pr}\right] \right. \\
& \left. - \sum_{q,r} \left[\Gamma_q \left(R_\varepsilon^{22}\right)_{pq} - Q_q \left(R_\varepsilon^{12}\right)_{pq}\right]\left[-\Gamma_r \left(R_\varepsilon^{11}\right)_{pr} - Q_r \left(R_\varepsilon^{21}\right)_{pr}\right] \right\}
\end{aligned}$$

$$
\begin{aligned}
&- \frac{1}{\varepsilon^2}\sum_q V_p V_q \Delta h_{qp}\eta^{\text{lap}}_{\varepsilon,pq} + \frac{V_p}{\varepsilon^2}\sum_{q,r} V_q V_r \big(h_q(s_r+s_q)\eta^{(1,0)}_{\varepsilon,qr} \\
&+ h_p(s_r+s_p)\eta^{(1,0)}_{\varepsilon,pr}\big)\eta^{(1,0)}_{\varepsilon,pq} + \frac{V_p}{\varepsilon^2}\sum_{q,r} V_q V_r \big(h_q(s_r+s_q)\eta^{(0,1)}_{\varepsilon,qr} \\
&+ h_p(s_r+s_p)\eta^{(0,1)}_{\varepsilon,pr}\big)\eta^{(0,1)}_{\varepsilon,pq} + \frac{1}{Re}\frac{1}{\varepsilon^2}\sum_{q,r}\Bigg\{\frac{V_p}{\rho_q}\Bigg[\frac{4}{3}(V_q Q_r + V_r Q_q)\eta^{(1,0)}_{\varepsilon,qr} \\
&- (V_q\Gamma_r + V_r\Gamma_q)\eta^{(0,1)}_{\varepsilon,qr}\Bigg] + \frac{V_q}{\rho_p}\Bigg[\frac{4}{3}(V_p Q_r + V_r Q_p)\eta^{(1,0)}_{\varepsilon,pr} \\
&- (V_p\Gamma_r + V_r\Gamma_p)\eta^{(0,1)}_{\varepsilon,pr}\Bigg]\Bigg\}\eta^{(1,0)}_{\varepsilon,pq} + \frac{1}{Re}\frac{1}{\varepsilon^2}\sum_{q,r}\Bigg\{\frac{V_p}{\rho_q}\Bigg[\frac{4}{3}(V_q Q_r + V_r Q_q)\eta^{(0,1)}_{\varepsilon,qr} \\
&+ (V_q\Gamma_r + V_r\Gamma_q)\eta^{(1,0)}_{\varepsilon,qr}\Bigg] + \frac{V_q}{\rho_p}\Bigg[\frac{4}{3}(V_p Q_r + V_r Q_p)\eta^{(0,1)}_{\varepsilon,pr} \\
&+ (V_p\Gamma_r + V_r\Gamma_p)\eta^{(1,0)}_{\varepsilon,pr}\Bigg]\Bigg\}\eta^{(0,1)}_{\varepsilon,pq},
\end{aligned}
\tag{A.5c}
$$

$$
\frac{ds_p}{dt} = \frac{1}{Re}\frac{\Phi_p}{\rho_p h_p} + \frac{1}{RePr}\frac{1}{\rho_p h_p \varepsilon^2}\sum_q V_q \Delta h_{qp}\eta^{\text{lap}}_{\varepsilon,pq}, \tag{A.5d}
$$

$$
\frac{dV_p}{dt} = Q_p, \tag{A.5e}
$$

$$
\frac{dh_p}{dt} = -(\gamma-1)h_p\theta_p + \frac{\gamma}{Re}\frac{\Phi_p}{\rho_p} + \frac{\gamma}{RePr}\frac{1}{\rho_p\varepsilon^2}\sum_q V_q \Delta h_{qp}\eta^{\text{lap}}_{\varepsilon,pq}. \tag{A.5f}
$$

The viscous dissipation is computed as

$$
\begin{aligned}
\Phi_p = \frac{\Gamma_p^2}{V_p^2} + \frac{4}{3}\frac{Q_p^2}{V_p^2} - 2\Bigg\{&\sum_{q,r}\big[\Gamma_q\big(R^{21}_\varepsilon\big)_{pq} - Q_q\big(R^{11}_\varepsilon\big)_{pq}\big]\big[-\Gamma_r\big(R^{12}_\varepsilon\big)_{pr} - Q_r\big(R^{22}_\varepsilon\big)_{pr}\big] \\
&- \sum_{q,r}\big[\Gamma_q\big(R^{22}_\varepsilon\big)_{pq} - Q_q\big(R^{12}_\varepsilon\big)_{pq}\big]\big[-\Gamma_r\big(R^{11}_\varepsilon\big)_{pr} - Q_r\big(R^{21}_\varepsilon\big)_{pr}\big]\Bigg\}.
\end{aligned}
\tag{A.6}
$$

In the boundary zone, Eq. (A.5f) is replaced by the particle form of the boundary condition (24)

$$
\frac{dh_p}{dt} = -\frac{1}{R_p\varepsilon}\sum_{q,R_q<R_p} V_q \Delta h_{pq}\big(\eta^{R,(1,0)}_{pq}x_{p,1} + \eta^{L,(0,1)}_{pq}x_{p,2}\big) - \frac{h_p - \frac{1}{\gamma-1}}{2R_p}, \tag{A.7}
$$

where $R_p = |\mathbf{x}_p| = \sqrt{x_{p,1}^2 + x_{p,2}^2}$ and the notation $\eta^{L,(\alpha_1,\alpha_2)}$ indicates that the kernel is the left-sided kernel for approximating the (α_1, α_2) derivative. The linear combination of kernels is used to approximate the gradient in the local radial direction (see Fig. 1). Equation (A.7) holds for particles in the boundary zone, but the sum is over *all* particles, provided that $R_q < R_p$. This criterion is used to establish that the sum is over the inner half plane, as described in Section 3.1 and derived in [14]. Clearly this restriction corresponds to a circle rather than a half plane, and the intersection of this region with the kernel support

corresponds to a lens-shaped region rather than a semicircle, but the error is smaller than the leading-order error in the boundary condition itself. Equation (A.7) is supplemented by Eqs. (A.5a) (the boundary particles are allowed to move) and (A.5e). Γ_p, Q_p, and s_p are assumed constant in the boundary region.

ACKNOWLEDGMENTS

The first author gratefully acknowledges support under a NSF Graduate Research Fellowship. This research was supported in part by the National Science Foundation under Grant 9501349. A preliminary version of some of the work presented here was reported in [13].

REFERENCES

1. M. Abramowitz and I. A. Stegun, editors, *Handbook of Mathematical Functions*. American Mathematical Series (Natl. Bur. of Standards, Washington, DC, 1964).
2. C. Anderson and C. Greengard, On vortex methods, *SIAM J. Numer. Anal.* **22**(3), 413 (1985).
3. C. R. Anderson, A vortex method for flows with slight density variations, *J. Comput. Phys.* **61**, 417 (1985).
4. J. T. Beale and A. Majda, Vortex methods II: Higher order accuracy in two and three dimensions, *Math. Comput.* **39**(159), 29 (1982).
5. J. T. Beale and A. Majda, High order accurate vortex methods with explicit velocity kernels, *J. Comput. Phys.* **58**, 188 (1985).
6. A. J. Chorin, Numerical study of slightly viscous flow, *J. Fluid Mech.* **57**(4), 785 (1973).
7. B.-T. Chu and L. S. G. Kovásznay, Non-linear interactions in a viscous heat-conducting compressible gas, *J. Fluid Mech.* **3**, 494 (1958).
8. G.-H. Cottet, Artificial viscosity models for vortex and particle methods, *J. Comput. Phys.* **127**, 299 (1996).
9. G.-H. Cottet and P. Koumoutsakos, *Vortex Methods: Theory and Practice* (Cambridge Univ. Press, Cambridge, UK, 2000).
10. S. C. Crow, Aerodynamic sound emission as a singular perturbation problem, *Stud. Appl. Math.* **XLIX**(1), 21 (1970).
11. G. Daeninck, *Local Refinement in Lagrangian Vortex Particle Methods*, Master's thesis (Université Catholique de Louvain, 2000). Advised by G. S. Winckelmans.
12. P. Degond and S. Mas-Gallic, The weighted particle method for convection–diffusion equations, Part 1: The case of an isotropic viscosity, *Math. Comput.* **53**(188), 485 (1989).
13. J. Eldredge, T. Colonius, and A. Leonard, *A Vortex Particle Method for Compressible Flows*, AIAA Paper 2001–2641 (AIAA Press, Washington, DC, 2001).
14. J. D. Eldredge, A. Leonard, and T. Colonius, A general deterministic treatment of derivatives in particle methods, *J. Comput. Phys.*, in press.
15. B. Engquist and A. Majda, Absorbing boundary conditions for the numerical simulation of waves, *Math. Comput.* **31**(139), 629 (1977).
16. M. A. Epton and B. Dembart, Multipole translation theory for the three-dimensional Laplace and Helmholtz equations, *SIAM J. Sci. Stat. Comput.* **16**, 865 (1995).
17. D. Fishelov, A new vortex scheme for viscous flows, *J. Comput. Phys.* **86**, 211 (1990).
18. A. F. Ghoniem, A. J. Chorin, and A. K. Oppenheim, Numerical modelling of turbulent flow in a combustion tunnel, *Philos. Trans. R. Soc. London A* **304**, 303 (1982).
19. R. A. Gingold and J. J. Monaghan, Smoothed particle hydrodynamics: Theory and application to nonspherical stars, *Mon. Not. R. Astron. Soc.* **181**, 375 (1977).
20. D. Givoli, Non-reflecting boundary conditions, *J. Comput. Phys.* **94**, 1 (1991).
21. L. Greengard and V. Rokhlin, A fast algorithm for particle simulations, *J. Comput. Phys.* **73**(2), 325 (1987).

22. O. H. Hald, Convergence of vortex methods for Euler's equations, II, *SIAM J. Numer. Anal.* **16**, 726 (1979).
23. M. S. Howe, Contributions to the theory of aerodynamic sound, with application to excess jet noise and the theory of the flute, *J. Fluid Mech.* **71**(4), 625 (1975).
24. O. M. Knio, L. Collorec, and D. Juvé, Numerical study of sound emission by 2D regular and chaotic vortex configurations, *J. Comput. Phys.* **116**, 226 (1995).
25. P. Koumoutsakos, A. Leonard, and F. Pépin, Boundary conditions for viscous vortex methods, *J. Comput. Phys.* **113**, 52 (1994).
26. A. Krishnan and A. F. Ghoniem, Simulation of rollup and mixing in Rayleigh–Taylor flow using the transport-element method, *J. Comput. Phys.* **99**, 1 (1992).
27. L. D. Landau and E. M. Lifshitz, *Fluid Mechanics*, Course of Theoretical Physics, Vol. 6 (Pergamon, Elmsford, NY, 1959).
28. S. K. Lele, *Computational Aeroacoustics: A Review*, AIAA Paper 97-0018 (AIAA Press, Washington, DC, 1997).
29. A. Leonard, Vortex methods for flow simulation, *J. Comput. Phys.* **37**(3), 289 (1980).
30. M. V. Melander, N. J. Zabusky, and J. C. McWilliams, Symmetric vortex merger in two dimensions: Causes and conditions, *J. Fluid Mech.* **195**, 303 (1988).
31. B. E. Mitchell, S. K. Lele, and P. Moin, Direct computation of the sound from a compressible co-rotating vortex pair, *J. Fluid Mech.* **285**, 181 (1995).
32. W. Möhring, On vortex sound at low Mach number, *J. Fluid Mech.* **85**, 685 (1978).
33. W. Möhring, *Sound Generation From Convected Vortices*, unpublished, 1997.
34. J. J. Monaghan, Particle methods for hydrodynamics, *Comput. Phys. Rep.* **3**, 71 (1985).
35. J. J. Monaghan, On the problem of penetration in particle methods, *J. Comput. Phys.* **82**, 1 (1989).
36. J. J. Monaghan, SPH and Riemann solvers, *J. Comput. Phys.* **136**, 298 (1997).
37. J. J. Monaghan and R. A. Gingold, Shock simulation by the particle method SPH, *J. Comput. Phys.* **52**, 374 (1983).
38. E.-A. Müller and F. Obermeier, The spinning vortices as a source of sound, in *Proceedings of the Conference on Fluid Dynamics of Rotor and Fan Supported Aircraft at Subsonic Speeds*, AGARD CP-22 (NATO (AGARD) 1967), pp. 22.1–22.8.
39. K. P. Pothou, S. G. Voutsinas, S. G. Huberson, and O. M. Knio, Application of 3-d particle method to the prediction of aerodynamic sound, in *Vortex Flows and Related Numerical Methods II* European Series in Applied and Industrial Mathematics (Soc. de Math. Appl. & Industr., Paris, 1996), Vol. 1.
40. A. Powell, Theory of vortex sound, *J. Acoust. Soc. Am.* **36**(1), 177 (1964).
41. T. R. Quackenbush, A. H. Boschitsch, G. S. Winckelmans, and A. Leonard, *Fast Lagrangian Analysis of Three Dimensional Unsteady Reacting Flow with Heat Release*, AIAA Paper 96-0815 (AIAA Press, Washington, DC, 1996).
42. P. A. Raviart, An analysis of particle methods, in *Numerical Methods in Fluid Dynamics*, edited by F. Brezzi, Lecture Notes in Mathematics (Springer-Verlag, New York, 1983), Vol, 1127, pp. 243–324.
43. T. Sarpkaya, Computational methods with vortices—The 1988 Freeman Scholar Lecture, *J. Fluids Eng.* **111**, 5 (1989).
44. I. J. Schoenberg, *Cardinal Spline Interpolation* (Soc. for Industr. & Appl. Math., Philadelphia, 1973).
45. M. C. Soteriou and A. F. Ghoniem, On the effects of the inlet boundary condition on the mixing and burning in reacting shear flows, *Combust. Flame* **112**, 404 (1998).
46. S. V. Tsynkov, Numerical solution of problems on unbounded domains. A review, *Appl. Numer. Math.* **27**, 405 (1998).
47. G. S. Winckelmans and A. Leonard, Contributions to vortex particle methods for the computation of three-dimensional incompressible unsteady flows, *J. Comput. Phys.* **109**(2), 247 (1993).
48. J. E. Yates, *Application of the Bernoulli Enthalpy Concept to the Study of Vortex Noise and Jet Impingement Noise*, Technical Report CR-2987 (Natl. Aeronautics & Space Admin., Washington, DC, 1978).